Supporting Materials

Superior and Anti-fatigue Electro-strain in $Bi_{0.5}Na_{0.5}TiO_3$-based Polycrystalline Relaxor Ferroelectrics

Jie Yin[1], Gang Liu[1], Xiang Lv[1], Yuxing Zhang[1], Chunlin Zhao[1], Bo Wu[1,2], Xingmin Zhang[3], Jiagang Wu[1, a)]

[1]*Department of Materials Science, Sichuan University, 610064, Chengdu, P. R. China*

[2]*Sichuan Province Key Laboratory of Information Materials and Devices Application, Chengdu University of Information Technology, Chengdu, P. R. China*

[3]*Shanghai Synchrotron Radiation Facility, Shanghai Institute of Applied Physics, Chinese Academy of Sciences, Pudong New Area, Shanghai 201204, P. R. China*

a) Corresponding author:

Email: msewujg@scu.edu.cn and wujiagang0208@163.com

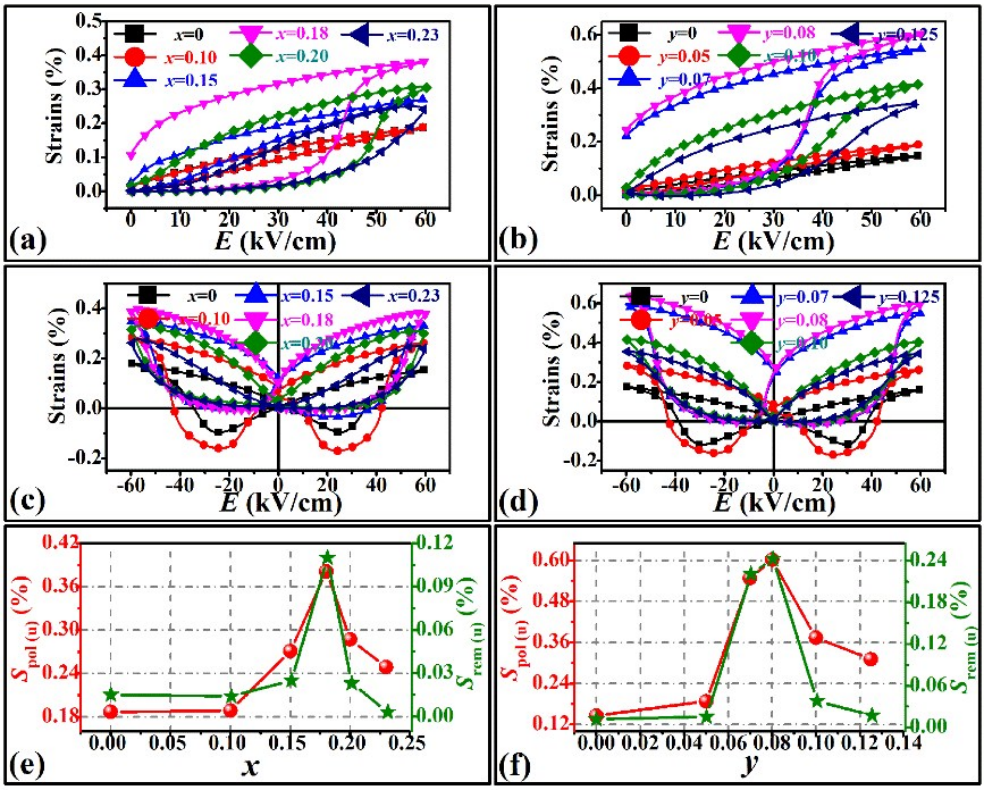

Figure S1. Materials selection part: (a), (b) Unipolar and (c), (d) bipolar electro-strain of $\{Bi_{0.5}[(Na_{0.80}K_{0.20})_{1-x}Li_x)]_{0.5}\}_{(1-y)}Sr_yTiO_3$ ceramics with different doped ions (x=Li^+, y=Sr^{2+}). Variations of unipolar poling strain $S_{pol(u)}$ and remnant strain $S_{rem(u)}$ against (e) Li^+ content (x) and (f) Sr^{2+} content (y).

To select the critical composition, the relationship between doping contents and corresponding electro-strain behaviors of $\{Bi_{0.5}[(Na_{0.80}K_{0.20})_{1-x}Li_x)]_{0.5}\}_{(1-y)}Sr_yTiO_3$ ceramics is studied, which is conducted under the E-field of 60 kV/cm, as displayed in Fig. S1. Both of the unipolar poling strain $S_{pol(u)}$ and the unipolar remnant strain $S_{rem(u)}$ first increase and then decrease with the increasing x contents (x/y=x/0.04), and $S_{pol(u)}$ reaches to the peak value of ~0.383 % for x/y=0.18/0.04 [Fig. S1e]. Similar tendency can be observed with increasing y contents (x/y=0.10/y), and the superior $S_{pol(u)}$ value of ~0.602 % is realized in the sample with x/y=0.10/0.08 [Fig. S1f]. Here, we can see

that composition engineering can lead to the disappearance of $S_{rem(u)}$, but it will significantly decrease the $S_{pol(u)}$ at the same time, leading to the overall inferior strain behaviors. Therefore, from a series of lithium- and strontium-doped BNT-BKT compositions, we select $[Bi_{0.5}(Na_{0.72}K_{0.18}Li_{0.10})_{0.5}]_{0.92}Sr_{0.08}TiO_3$ as the critical studied composition, because of its ultrahigh $S_{pol(u)}$ (0.602% @ 60 kV/cm) and sizeable $S_{pol(u)}$ (0.241% @ 60 kV/cm).

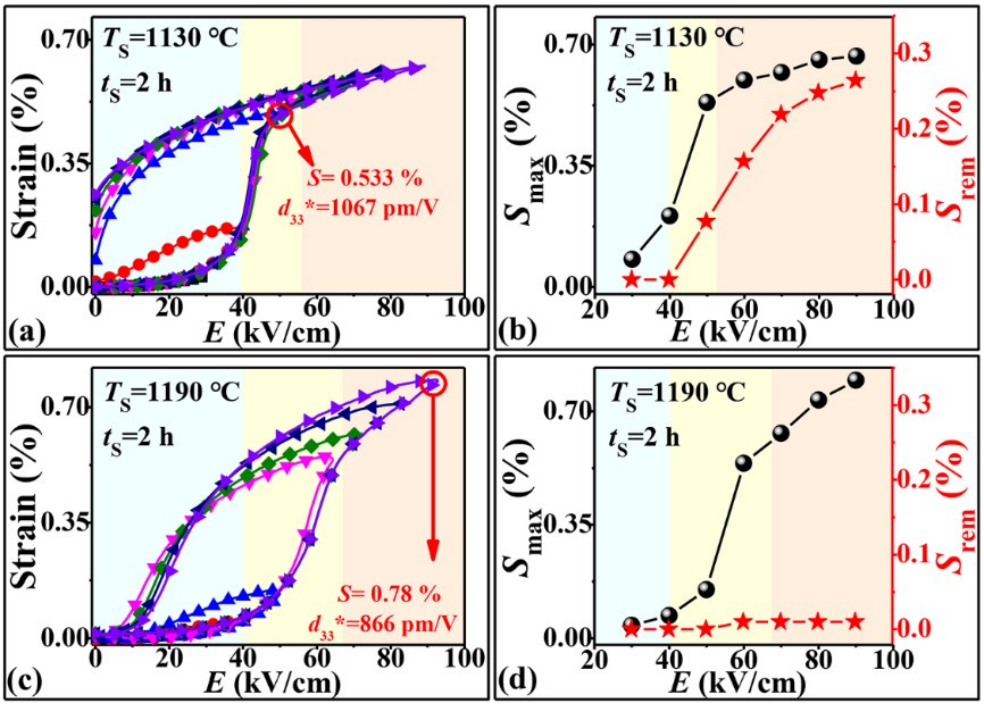

Figure S2. Large field unipolar electro-strain behaviors, part 1: Unipolar electro-strain behaviors and their maximum electro-strains S_{max} and d_{33}* values under different E-fields of $[Bi_{0.5}(Na_{0.72}K_{0.18}Li_{0.10})_{0.5}]_{0.92}Sr_{0.08}TiO_3$ samples prepared at (a), (b) T_S=1130 °C, t_S=2 h and (c), (d) T_S=1190 °C, t_S=2 h.

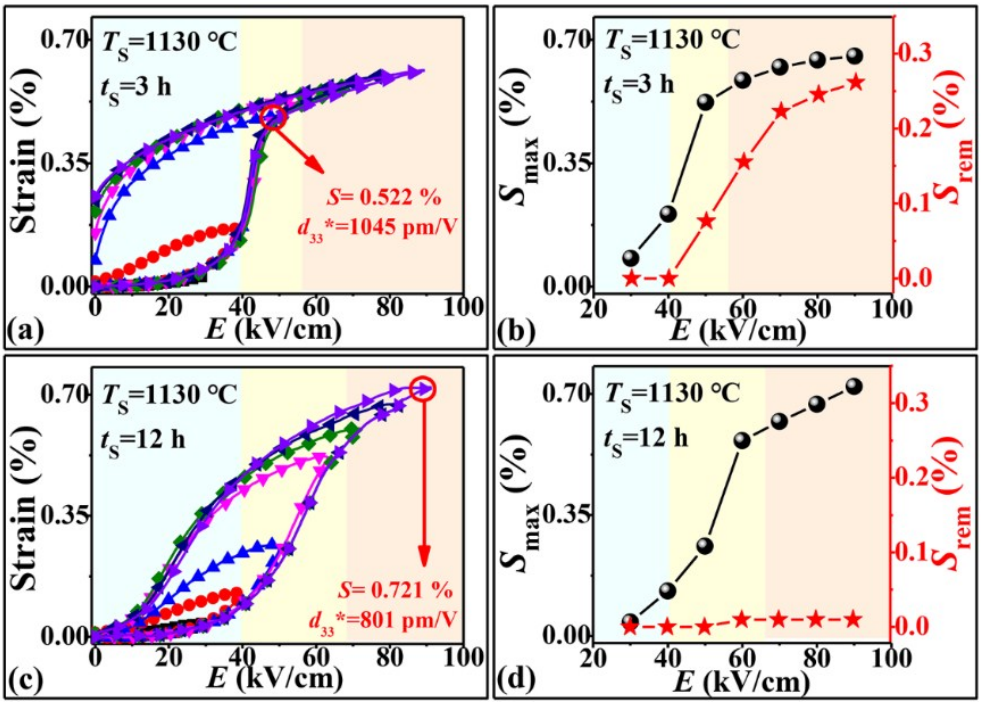

Figure S3. Large field unipolar electro-strain behaviors, part 2: Unipolar electro-strain behaviors and their maximum electro-strain S_{max} and d_{33}* values under different *E*-fields of $[Bi_{0.5}(Na_{0.72}K_{0.18}Li_{0.10})_{0.5}]_{0.92}Sr_{0.08}TiO_3$ samples prepared at (a), (b) T_S=1130 °C, t_S=3 h and (c), (d) T_S=1130 °C, t_S=12 h.

Figures S2 and S3 give the *E*-field-dependent unipolar electro-strain behaviors, measured with the samples prepared at different sintering conditions (T_S=1130 °C, t_S=2 h; T_S=1190 °C, t_S=2 h and T_S=1130 °C, t_S=3 h; T_S=1130 °C, t_S=12 h). For samples sintered at T_S=1130 °C, t_S=2 h, their d_{33}* values reach the maximum value (~1067 pm/V) at 50 kV/cm [Figs. S2a, b]. Particularly, an even higher electro-strain value of 0.78 % at 90 kV/cm can be obtained in the samples sintered at T_S=1190 °C, t_S=2 h [Figs. S2c, d]. For samples sintered with prolonged sintering time, similar trend can be observed, as shown in Figs. S3a-d. Since BNT-based ceramics undergo the field-induced relaxor-ferroelectric transition, the ferroelectric-like strain responses can be found under the higher electric field ($E \geq 60$ kV/cm). Notably, when we elevate the

sintering temperatures T_S or prolong the sintering keeping time t_S, electro-strain responses still share a relatively rapid growth, which will be discussed in our main text.

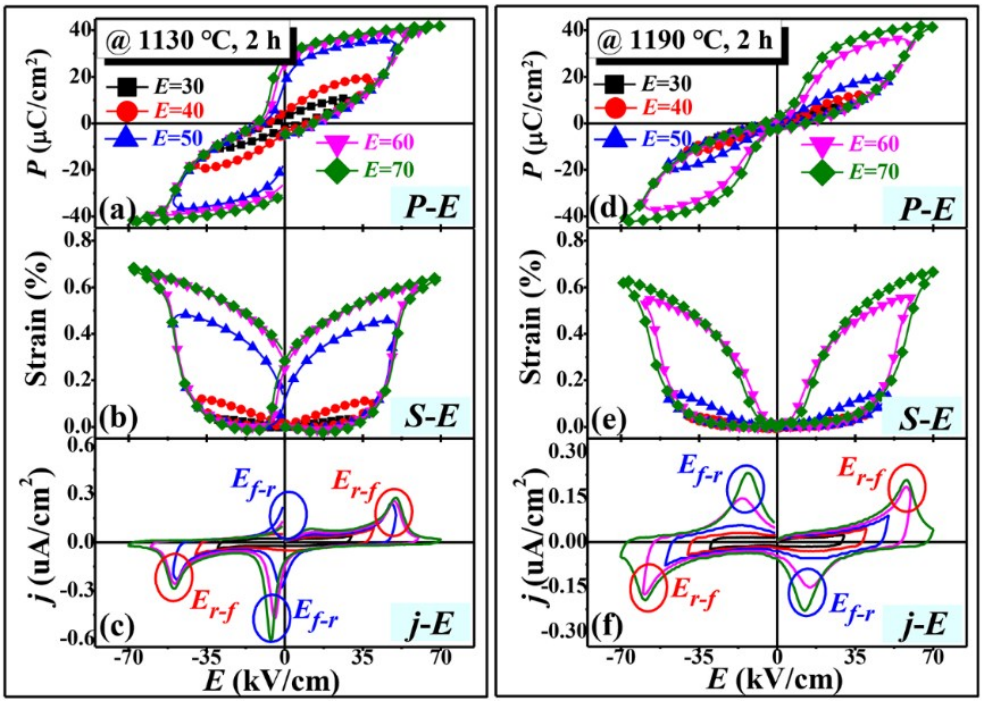

Figure S4. Large field bipolar ferroelectric behaviors, part 1: Polarization, electro-strains and current density versus electric-field (*P-E*, *S-E* and *j-E*) curves for $[Bi_{0.5}(Na_{0.72}K_{0.18}Li_{0.10})_{0.5}]_{0.92}Sr_{0.08}TiO_3$ samples prepared at (a)-(c) T_S=1130 ℃, t_S=2 h and (d)-(f) T_S=1190 ℃, t_S=2 h.

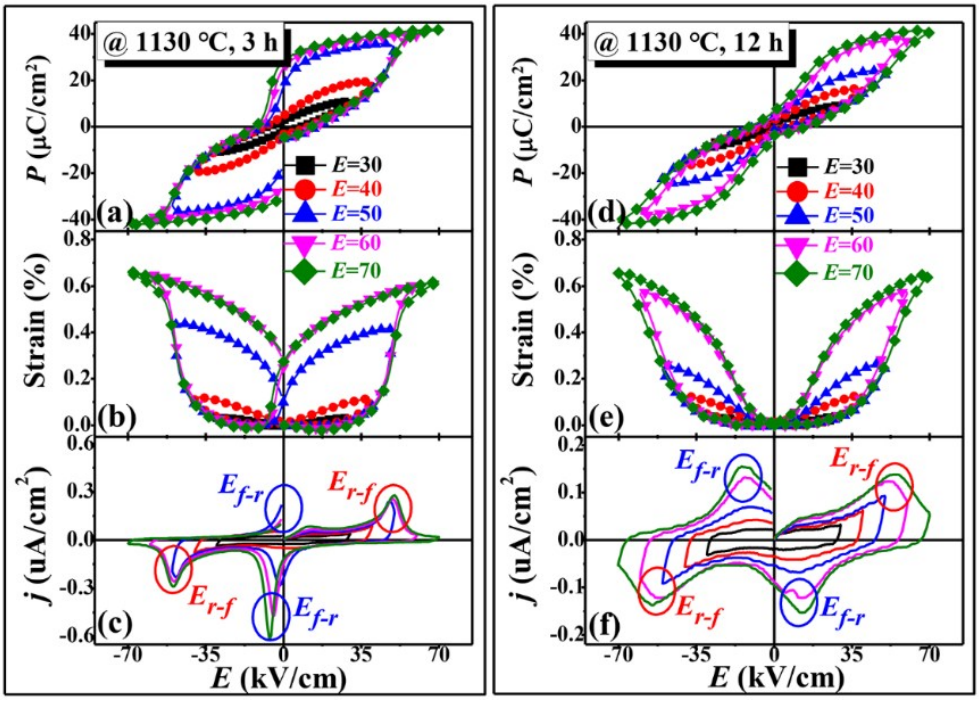

Figure S5. Large field bipolar ferroelectric behaviors, part 2: Polarization, electro-strains and current density versus electric-field (*P*-*E*, *S*-*E* and *j*-*E*) curves for $[Bi_{0.5}(Na_{0.72}K_{0.18}Li_{0.10})_{0.5}]_{0.92}Sr_{0.08}TiO_3$ samples prepared at (a)-(c) T_S=1130 ℃, t_S=3 h and (d)-(f) T_S=1190 ℃, t_S=12 h.

To reflect the transitions between FE phase and RE state [1], large *E*-field-dependent *P*-*E*, *S*-*E* and *j*-*E* loops of representative samples (T_S=1130 ℃, t_S=2 h, T_S=1190 ℃, t_S=2 h and T_S=1130 ℃, t_S=3 h, T_S=1130 ℃, t_S=12 h) are given, as shown in Figs. S4 and S5. The rapid rise of polarization [Figs. S4a, S4d and S5a, S5d] and the rapid rise of electro-strain [Figs. S4b, S4e and S5b, S5e] directly associate with the RE to FE phase transition [Figs. S4c, S4f and S5c, S5f], while the rapid fall of polarization [Figs. S4a, S4d and S5a, S5d] and the rapid fall of electro-strain [Figs. S4b, S4e and S5b, S5e] directly associate with the FE to RE phase transition [Figs. S4c, S4f and S5c, S5f]. Notably, by elevating the sintering temperature T_S or prolonging the sintering keeping

time t_S, the FE to RE transition happens in advance before the *E*-field goes down to zero.

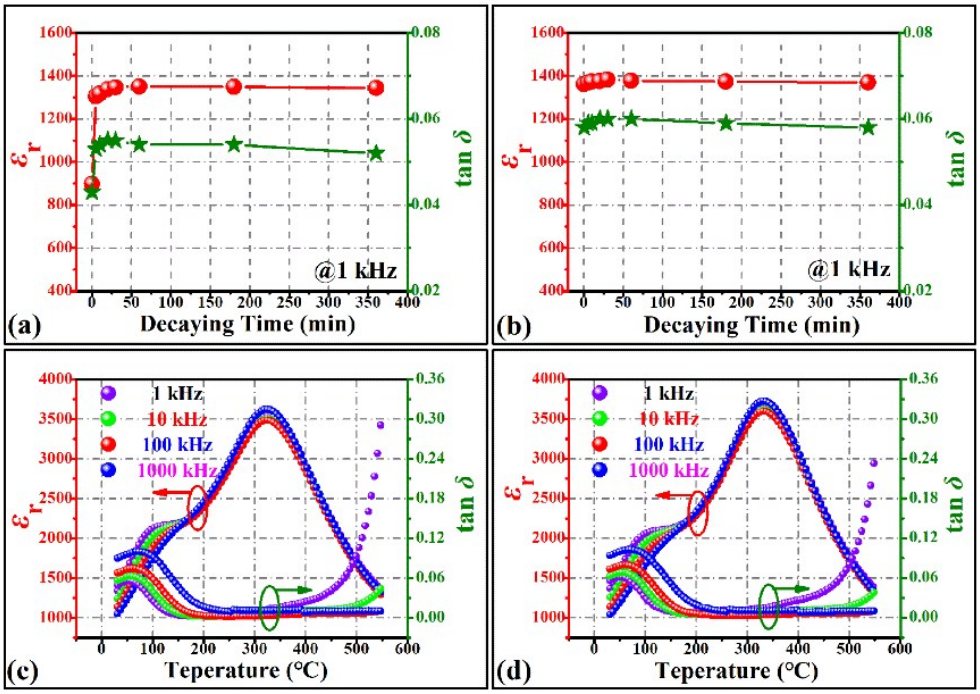

Figure S6. Decaying time-dependent dielectric behaviors part: (a), (b) Decaying time-dependent relative dielectric constant (ε_r) and loss tangent (tan δ) of poled $[Bi_{0.5}(Na_{0.72}K_{0.18}Li_{0.10})_{0.5}]_{0.92}Sr_{0.08}TiO_3$ samples measured at 1kHz. (c), (d) Temperature-dependent relative dielectric constant (ε_r) and loss tangent (tan δ) of poled $[Bi_{0.5}(Na_{0.72}K_{0.18}Li_{0.10})_{0.5}]_{0.92}Sr_{0.08}TiO_3$ samples measured at 1k, 10k, 100k, 1000kHz. Data shown in (a), (c) are collected from samples sintered at T_S=1130 ℃, t_S=2 h, while data shown in (b), (d) are collected from samples sintered at T_S=1130 ℃, t_S=12 h.

Figure S6 shows the decaying time-dependent and temperature-dependent dielectric behaviors of $[Bi_{0.5}(Na_{0.72}K_{0.18}Li_{0.10})_{0.5}]_{0.92}Sr_{0.08}TiO_3$ samples. Interestingly, for samples sintered at T_S=1130 ℃, t_S=2 h [Fig. S6a], their relative dielectric constant (ε_r) and loss tangent (tan δ) have somewhat lower values when the samples are just poled (decaying

time=0 min), which will get a rapid increase at first (0 min≤decaying time≤5 min) and get flattened at last (decaying time≥30 min). However, for samples sintered at T_S=1130 ℃, t_S=12 h [Fig. S6b], flattened variations can be observed with the increasing decaying time. The rapid increase of dielectric responses can be seen as the faded ferroelectricity in BNT-based relaxor ferroelectrics, which will be found in the discussions in our main text. From Figs. S6c and S6d, one can see that all samples exhibit diffused and frequency dispersive peaks. As the frequency increases, their ε_r values decreases and their maximums are slightly shifted towards higher temperatures. In addition, their ε_r values show a pronounced dependence on the frequencies when T≤200 ℃. All these characteristics further demonstrate the relaxor nature of BNT-based samples in this work.

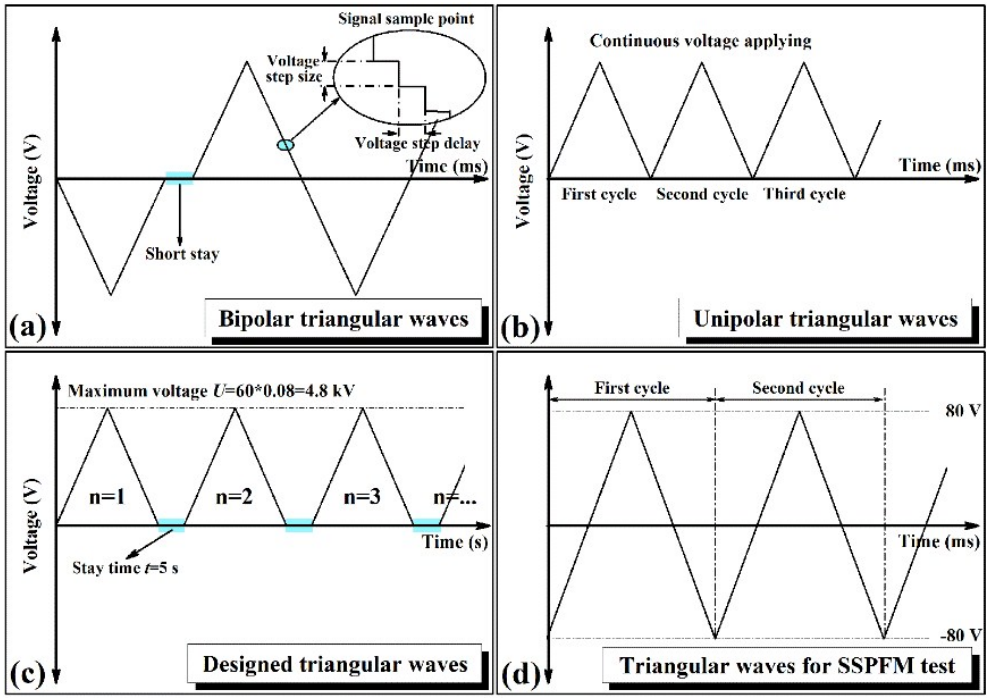

Figure S7. Test waves part: (a) Bipolar triangular waves utilized to study the bipolar ferroelectric responses, (b) unipolar triangular waves utilized to study the cyclic unipolar electro-strain behaviors, (c) designed triangular waves utilized to study the

relaxation mechanisms and (d) triangular waves utilized for the local SSPFM test.

Figure S7 gives the typical test waves applied in this work. Notably, unlike the fatigue tests, to better study the relaxation process of the *E*-field-induced ferroelectric state, a short stay time (t=5 s) was introduced at the interval between the adjacent voltage signal [Fig. S7c].

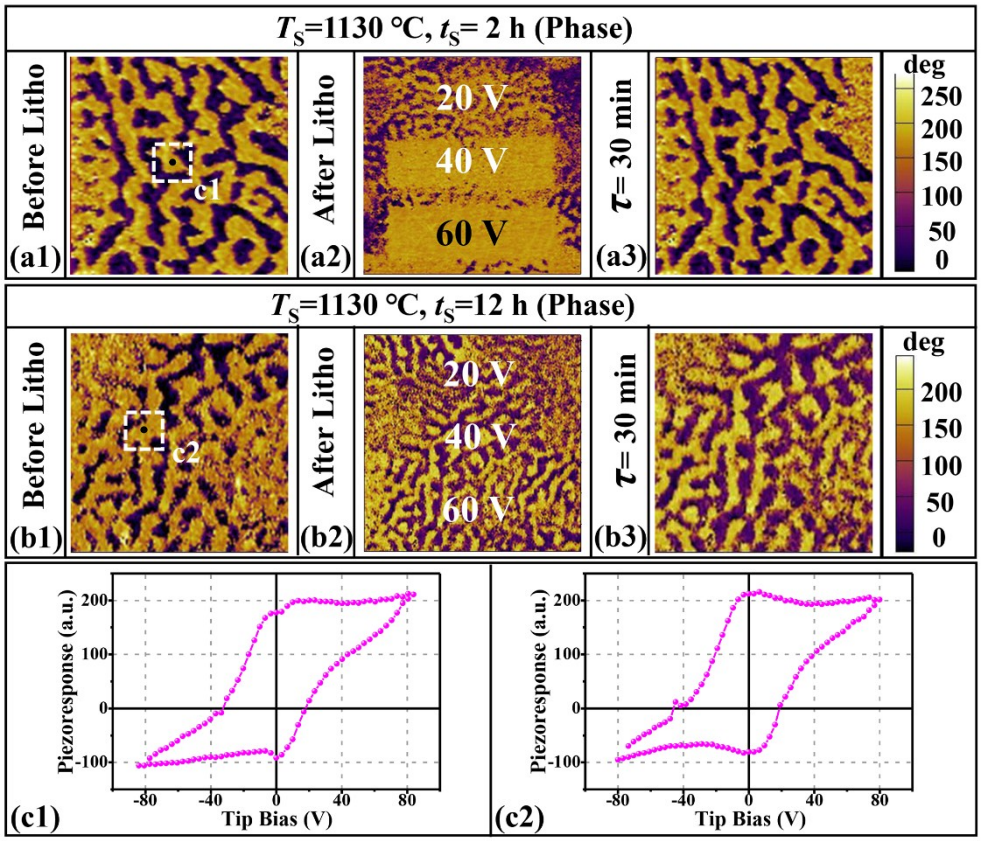

Figure S8. Local domain morphology and local piezo-response part: Out-of-plane (OP) PFM phase images for the samples sintered at a) T_S=1130 ℃, t_S=2 h and b) T_S=1130 ℃, t_S=12 h. a1), b1) Before the local poling (litho) process, the drive voltage of 3 V was applied to record the original domain morphology of a 1 × 1 μm^2 area. During the local poling (litho) process, to visualize the display, a negative DC voltage (60 V) was first applied to the tip during the scanning of a 2 × 2 μm^2 area. Then, a

positive DC voltage with different values (20, 40 and 60 V), depending on the scanning areas, was applied to the tip during the scanning of a 1.5 × 0.5 μm^2 area. (a2), (b2) After the local poling (litho) process, the drive voltage of 3 V was immediately applied to record the instantaneous domain morphology. (a3), (b3) After the relaxation time (t) of 30 minutes, the drive voltage of 3 V was applied to record the domain morphology after the relaxation process. (c1), (c2) Typical butterfly loops and phase hysteresis loops measured at local positions (-80 V ≤ the swept voltage V ≤ 80 V), where data of (c1) are measured from the dot shown in (a1) and data of (c2) are measured from the dot shown in (b1).

Figure S8 gives the local piezo-response behaviors of the samples prepared at different sintering conditions (T_S=1130 ℃, t_S=2 h; T_S=1130 ℃, t_S=12 h), which is the supplementary part of PFM tests shown in our main text.

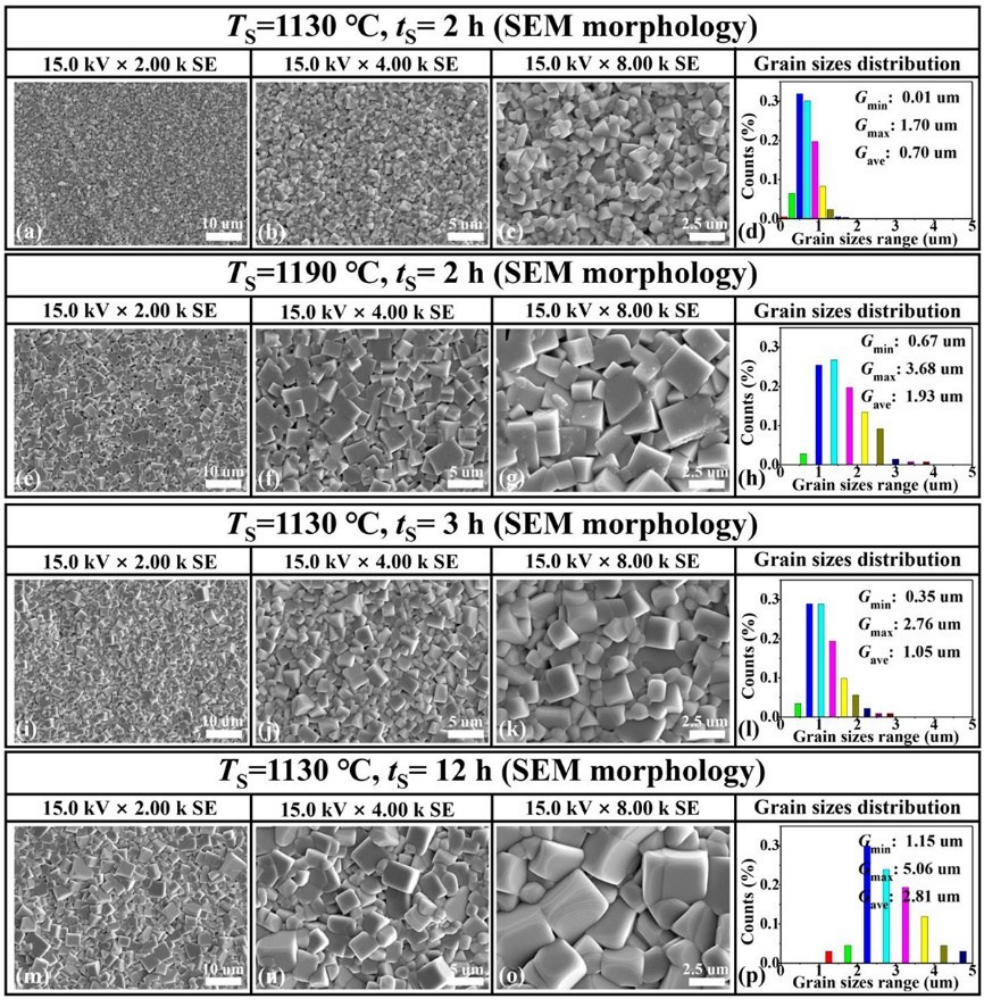

Figure S9. Microstructure part: Grain morphology and grain sizes distribution of the prepared samples sintered at sintering temperatures (a-d) T_s=1130 ℃, (e-h) 1190 ℃ with the same sintering keeping time t_s=2 h and sintering keeping time (i-l) t_s=3 h, (m-p) t_s=12 h with the same sintering temperature T_s=1130 ℃.

FE-SEM images and corresponding grain sizes distribution analysis of the samples prepared at representative sintering conditions are given in Fig. S9. Grains of all samples exhibit the neat rectangular shapes with clear grain boundaries, and grain sizes of these samples exhibit an obviously dependence on the sintering conditions. When we elevate the sintering temperature T_s or prolong the sintering keeping time t_s, grains

come to be larger.

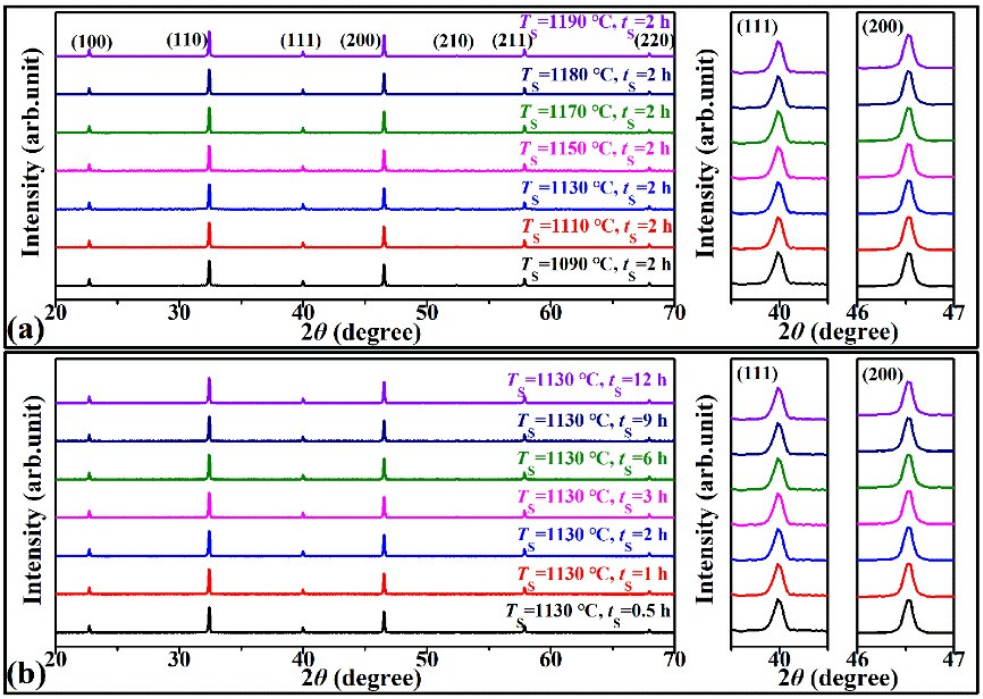

Figure S10. Average phase structure part: Normal XRD patterns of the critical composition samples prepared at (a) different sintering temperatures (t_s=2 h, different T_s) and (b) different sintering keeping time (T_s=1130 ℃, different t_s).

XRD patterns of unpoled critical composition samples prepared at different sintering conditions are shown in Fig. S10. All samples possess a typical perovskite phase, indicating that the average structure of this homogeneous solid solution has not been affected by sintering regulations. As can be seen in their expanded XRD patterns, all samples exhibit a pseudocubic structure without any obvious splitting peaks near 40° [indexed by (111)] and 46.5° [indexed by (200)], which belongs to be a characteristic of relaxor ferroelectrics [2].

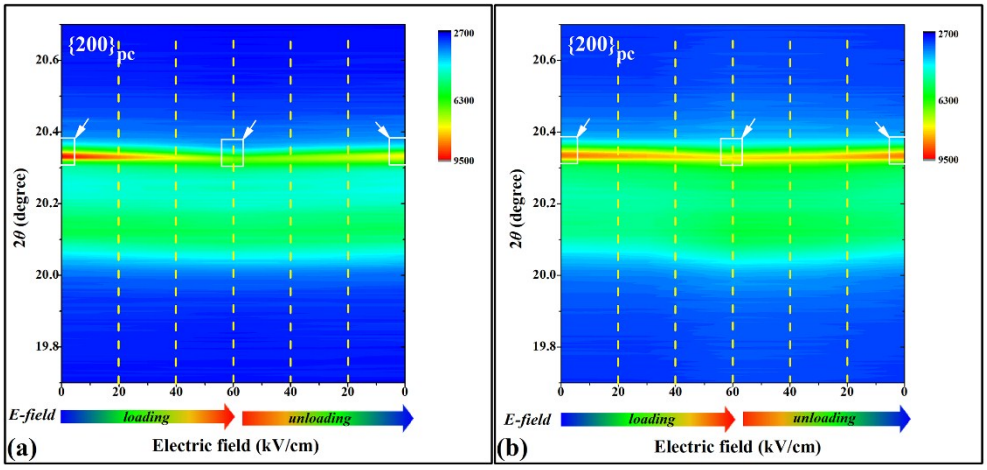

Figure S11. *E*-field-dependent average phase structure part: In-situ *E*-field induced characteristic $\{200\}_{pc}$ peak evolutions of the samples sintered with (a) T_S=1130 ℃, t_S=2 h and (b) T_S=1130 ℃, t_S=12 h.

Figures S11a and S11b show the *E*-field dependent in-situ characteristic $\{200\}_{pc}$ peak variations for the representative samples, corresponding to the $\{111\}_{pc}$ peak variations shown in our main text. Discrepancies can be found between the high-field state and the initial state [as marked in Figs. S11a and S11b], giving evidence for a macroscopically structural distortion. After removing the *E*-field completely, *E*-field-induced structural distortions can be partly kept [obvious discrepancies between the ultimate and the initial state, as marked in Fig. S11a] for the samples sintered with the shorter t_S [Fig. S11a], while almost no remnant structural distortions [no obvious discrepancies between the ultimate and the initial state, as marked in Fig. S11b] can be observed for the samples sintered with a longer t_S [Fig. S11b].

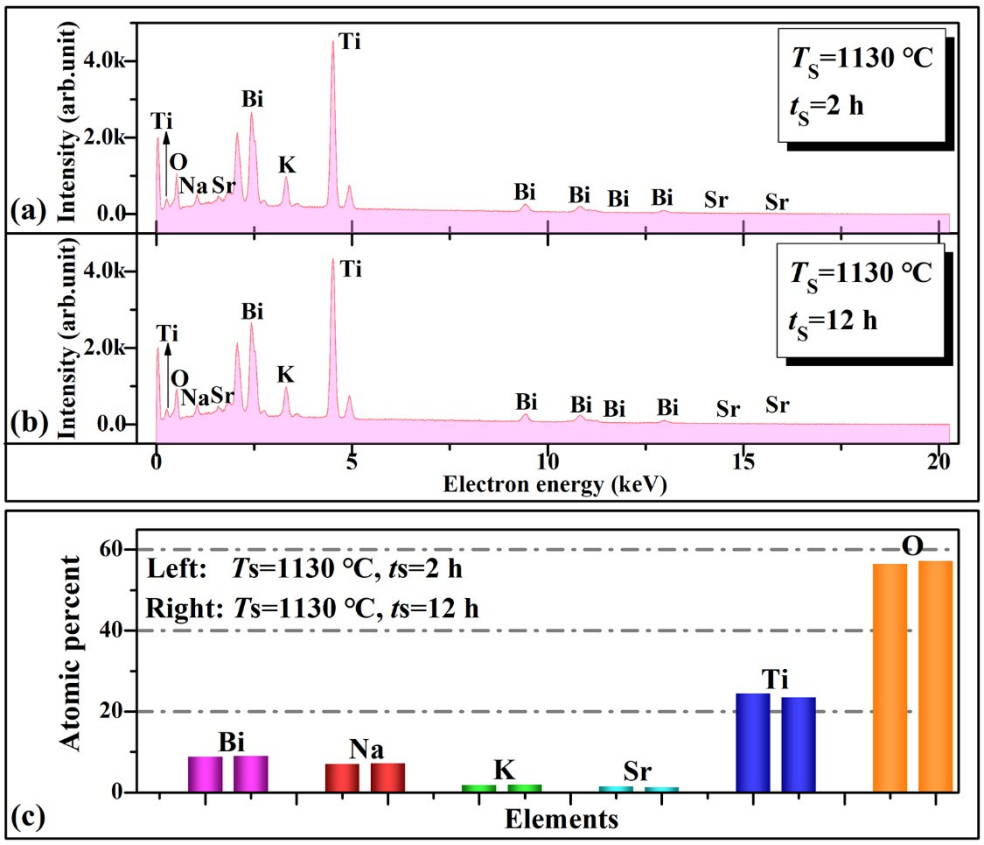

Figure S12. Elemental composition part: (a), (b) EDS patterns and (c) the corresponding elements ratios of the representative samples. Note here that the samples are polished to have a fair comparison of elements distribution.

In order to check the elements segregation condition of the samples sintered at T_s=1130 ℃, t_s=2 h and T_s=1130 ℃, t_s=12 h, energy dispersive spectrometer (EDS) analysis is given in Figs. S12a and S12b. EDS patterns indicate the existence of six elements (Bi, Na, K, Sr, Ti, O) in samples sintered at different sintering conditions, detailed data of which can be found in Tabs. S1 and S2. Figs. S12c gives the direct elements comparison of samples sintered at different sintering conditions, demonstrating that prolonged sintering time has little effects on elements proportion of the prepared samples.

Table S1: EDS data of samples prepared at sintering temperature T_s=1130 ℃ and sintering keeping time t_s=2 h

Elements	Type of lines	*wt* %	Atomic percent	Labels of standard samples	Standard of manufactures
O	K Lines	21.13	56.51	SiO_2	Yes
Na	K Lines	3.74	6.97	Albite	Yes
K	K Lines	1.65	1.81	KBr	Yes
Ti	K Lines	27.33	24.43	Ti	Yes
Sr	L lines	2.93	1.43	SrF_2	Yes
Bi	M lines	43.22	8.85	Bi	Yes
Total amount	/	100.00	100.00	/	/

Table S2: EDS data of samples prepared at sintering temperature T_s=1130 ℃ and sintering keeping time t_s=12 h

Elements	Type of lines	*wt* %	Atomic percent	Labels of standard samples	Standard of manufactures
O	K Lines	21.45	57.22	SiO_2	Yes
Na	K Lines	3.84	7.13	Albite	Yes
K	K Lines	1.73	1.89	KBr	Yes
Ti	K Lines	26.35	23.50	Ti	Yes
Sr	L lines	2.61	1.27	SrF_2	Yes
Bi	M lines	44.02	8.99	Bi	Yes
Total amount	/	100.00	100.00	/	/

Table S3. Detailed measured densities of all ceramic samples synthesized at different sintering conditions.

***Sintering temperature* (℃)**	***Sintering soaking time* (h)**	***Measured density (g/cm^3)***
1090	2	5.41
1110	2	5.56
1130	2	5.63
1150	2	5.57
1170	2	5.54
1180	2	5.58
1190	2	5.55
1130	0.5	5.24
1130	1	5.49
1130	3	5.58
1130	6	5.6
1130	9	5.51
1130	12	5.44

References

[1] J. Yin, C. L. Zhao, Y. X. Zhang and J. G. Wu, *J. Am. Ceram. Soc.*, 2017, **100**, 5601-5609.

[2] Wang, K.; Hussain, A.; Jo, W.; Rödel, J. Temperature-Dependent Properties of $(Bi_{1/2}Na_{1/2})TiO_3$–$(Bi_{1/2}K_{1/2})TiO_3$–$SrTiO_3$ Lead-Free Piezoceramics. *J. Am. Ceram. Soc.* **2012**, *95*(7), 2241-2247.